Nonlinear dynamics of shape memory alloy oscillators in tuning structural vibration frequencies

Linxiang Wang [a], Roderick V.N. Melnik [b,c,d,∗]

[a] The State Key Laboratory of Fluid Power Transmission and Control, Department of Ocean Science and Engineering, Zhejiang University, Hangzhou 310058, PR China
[b] M²NeT Laboratory, Wilfrid Laurier University, Waterloo, ON, Canada N2L 3C5
[c] Basque Excellence Research Center BCAM, Alameda Mazarredo, 14, 48009 Bilbao, Spain
[d] IKERBASQUE, Basque Foundation for Science, Alameda Urquijo, 36-5, 48011 Bilbao, Spain

ARTICLE INFO

ABSTRACT

Shape memory alloy (SMA) is one of the novel advanced functional materials that has an increasing range of current and potential applications, including smart materials and structures, bio-medical and nano-technologies. This range includes also applications of SMA for control and vibration tuning of various structures, seismic response mitigation, and others. In vibration tuning in many of these applications, it is often necessary to apply supplementary oscillators to absorb the vibration energy input into the primary system. Moreover, when supplementary oscillators are used in these applications, we often have to deal with a situation where the primary vibration frequency is not known a priori. In such cases, we have to design a robust supplementary oscillator such that it is able to operate in a rather wide range of frequencies. A SMA-based oscillator is an ideal candidate for these purposes. In the present paper, we propose a dynamic nonlinear model and its numerical realization for using SMA oscillators as vibration absorbers. The system under consideration consists of a SMA rod and an end-mass. We demonstrate that due to the thermo-mechanical coupling, the vibration characteristics of the supplementary oscillator can be tuned by changing its temperature. The dynamic nonlinear model of the SMA oscillator is simplified for the vibration analysis and an efficient numerical methodology is proposed to evaluate the performance of the oscillator. It is demonstrated that the vibration of the primary system can be tuned within a rather wide frequency range by using the SMA oscillator. It is also shown that at high temperatures the performance of the oscillator is close to that of a linear oscillator, while at low temperatures, the SMA oscillator behaves as a regular damper by using its dissipation due to mechanically-induced phase transformations.

© 2012 Elsevier Ltd. All rights reserved.

1. Introduction

Analysis and suppression of forced vibrations is an important problem in science and technology. Its effective solution helps us reduce noise, control resonance, and prevent structural failures. In doing so, it is often desirable to attenuate or completely suppress the vibrations. Among many existing approaches to this problem solution, the implementation of dynamic vibration absorbers is probably the simplest, yet one of the most popular, approach [1,2]. The principle of the dynamic vibration absorber is based on the absorption of vibration energy from the primary system and storing it via its own vibrations which, as a consequence, will reduce the vibration of the primary system. When the excitation frequency is close to the natural frequency of the primary system, and is known, the dynamic vibration absorber can be easily implemented by a linear mass-spring oscillator, as sketched in the left part of Fig. 1. Such an oscillator is able to suppress the vibration of the primary system completely.

1.1. Adaptive oscillators and shape memory alloys

The limitation of the linear mass-spring oscillator used for the vibration absorption and in similar technological applications lies with the fact that it only works when the excitation frequency is known and close (or, ideally, equal) to the natural frequency of the primary system. For many engineering structures, both such frequencies might not be known a priori [1,3,2]. In such cases, adaptive oscillators with adjustable stiffness [4] would be beneficial in order to tune (and ultimately to control) the vibrations so that the natural frequency of the oscillator can be adjusted to match the resonance frequency of the primary system [1]. Due to their thermo-mechanical coupling properties, shape memory

∗ Corresponding author at: M²NeT Laboratory, Wilfrid Laurier University, Waterloo, ON, Canada N2L 3C5. Tel.: +1 519 884 0710x3662; fax: +1 519 884 9738.
 E-mail address: rmelnik@wlu.ca (R.V.N. Melnik).
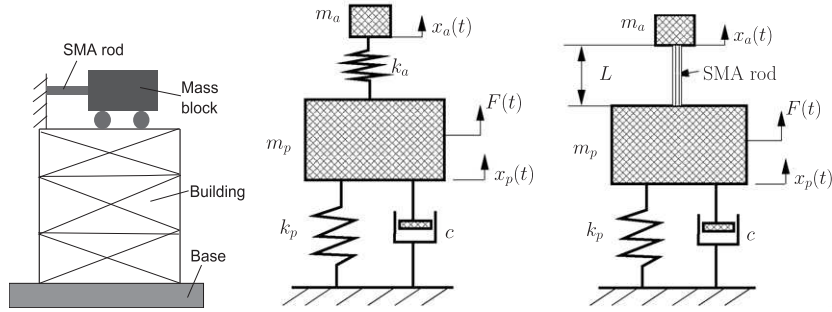
Fig. 1. Sketch of dynamic vibration absorbers: left – a SMA oscillator in building vibration suppression; centre – a linear mass vibration absorber; right – a SMA based vibration absorber.

alloys (SMAs) are promising materials for these purposes. These advanced materials have already been applied to the adaptive vibration absorption [5,3,6–8]. The unique properties of SMA lead to hardening the elastic modulus of the material at higher temperature (in the austenite state) and to its softening at lower temperature (in the martensite state). When the temperature is continuously adjusted, the elastic modulus of the material will be changing accordingly. Therefore, the thermo-mechanical coupling of SMAs provides a way to adjust the frequency response of vibration absorbers for adaptive vibration tuning [9–12]. Previous results on the technological applications of SMA (composite) beams showed that the frequency of the oscillator using such beams can be adjusted in a range of 15% [5,7,8].

1.2. Complex dynamics vs mono- and harmonic frequencies

Up to date, most studies in his field relied on mono-frequency or harmonic assumptions. If one considers the vibration tuning in more realistic situations, where the excitation frequencies may not necessarily be mono-frequency or harmonic and the primary system itself may be nonlinear, then the adaptive vibration absorber designed according to the standard frequency analysis might not be a suitable choice. Indeed, in this case vibration tuning should be implemented by taking energy dissipation into account, ensuring stability and robustness of the system, because of the energy dissipation driven vibration attenuation. Therefore, in addition to the thermo-mechanical coupling which has been taken into account in previous studies, it is also important to account in the developed models for another property of the SMAs associated with the hysteresis effects due to the first order martensitic phase transformations at low temperature, and austenite–martensite transformations at intermediate temperatures.

For the energy dissipation purpose, the SMA material can be switched between multiple martensite variants by external loadings at low temperature, as a result of induced martensite transformations. During such switchings, the external energy input into the material will be dissipated without an automatic recovery mechanism when it is unloaded, since all the martensite variants are energetically equivalent [20,14]. When the material temperature is around the value where martensite and austenite may coexist [15], transformations between martensite and austenite can be induced by external loadings. Input energy will also be dissipated, but only partly, while the other parts will be stored in the material via elastic deformations (see also [16]). When the material is unloaded, the stored energy can be recovered [17,9,18].

In order to exploit the application potential of SMAs in vibration tuning and similar applications, in this contribution we take into account both key SMA properties: the thermo-mechanical coupling and the hysteresis induced by phase transformations. The main ideas are explained in the next sections on an example of an idealized SMA rod with an end-mass as a vibration absorber [19]. For the vibration analysis, the SMA rod is modelled as a nonlinear spring with its stiffness dependent on temperature. In order to quantify the thermo-mechanical coupling and nonlinearities of constitutive laws for such a SMA oscillator, we apply the modified Ginzburg–Landau theory [20–22]. This allows us to model effectively the dynamical response of the SMA rod by simplifying the derived model to a nonlinear algebraic equation which gives the force–deformation relation of the oscillator. We provide details on the constitutive relation for the SMA rod, hysteresis due to martensite transformations, and austenite–martensite transformations, followed by a brief discussion of possible implications for the associated technologies.

2. Nonlinear vibrations of SMA: coupling primary and adaptive systems

The principle of applying a SMA oscillator as a vibration absorber is very similar to that of a linear oscillator, as shown in Fig. 1. The oscillator consists of an elastic component and an attached end-mass where in our case the elastic component is replaced by a SMA rod. The characteristics of the rod should be such that we can adjust its length and cross-sectional area accordingly to avoid buckling effects. The first results on the models for tuning vibration frequencies with SMA oscillators based on the modified Ginzburg–Landau theory appeared in [19]. Later, several other researchers looked at this problem (e.g., [23] and references therein). While in most of these papers the authors were essentially using the original Fremond's model, the current paper is a further development of models based on the modified Ginzburg–Landau theory [24]. Such models have a number of advantages compared to the previously developed models. They are much simpler, allowing greater flexibility in their usage for diverse engineering applications. If phase transformation induced dissipation is included into the model, the analysis of vibration attenuation was already carried out in [25]. These ideas appeared to be also useful in the analysis of phase transformations in nanotechnological and other applications [26].

To model the vibration tuning, the vibration of the primary system and the attached oscillator should be considered simultaneously. To do so, we formulate the governing equations for the entire system as follows:

$$m_p \ddot{x}_p + c_p \dot{x}_p + k_p x_p + F_s(x_p - x_a) = F(t),$$
$$m_a \ddot{x}_a = F_s(x_p - x_a),$$

(1)

where x_p and x_a are displacements of the primary and attached mass blocks, m_p and m_a, respectively, c_p is the friction coefficient and k_p is the spring stiffness in the primary system. The primary system is subject to an excitation input $F(t)$ which might be decomposed into harmonic components. The nonlinear restoring force produced by the SMA rod is denoted by F_s. It is a general nonlinear

function of deformation $x_p - x_a$ in the above equation. This can be easily generalized further by replacing the linear spring restoring force $k_p x_p$ with a nonlinear force.

If both the restoring forces in the primary system and the attached oscillator are linear, which is the case in the left part of Fig. 1, the displacement x_p can be obtained by using the following transfer function:

$$\frac{X_p(j\omega)}{F(j\omega)} = \frac{k_a - m_a\omega^2}{(-m_p\omega^2 + jc_p\omega + k_p + k_a)(-m_a\omega^2 + k_a) - k_a^2}, \qquad (2)$$

where ω is the frequency of the mono-frequency excitation force. If ω is close or equal to the natural frequency of the primary system, it will induce resonance. The vibration absorber can be designed to completely suppress the vibration by setting the modulus of the transfer function to zero. Formally, this can be attained by setting $k_a = m_a\omega^2$.

As mentioned earlier, in many technological applications the natural frequency of the primary system ω is not known a prior, it can also float in operation. Therefore, in designing the attached system we want to have the capability of changing its stiffness k_a in operation such that the vibration of the primary system can still be tuned when its natural frequency is changed. The thermo-mechanical coupling property of SMA makes this advanced material very suitable for this purpose, since its elastic modulus can be changed by changing its temperature. Furthermore, the material itself is inherently dissipative due to the hysteretic stress–strain relation, which makes it very useful for vibration suppression. Practically, the material temperature can be increased relatively fast via one of the available heating technologies, but the cooling rate is problematic for fast response [3,11,27]. Depending on the size and design of the devices, the material can be cooled by using heat sinking, or forced air/liquid, but its response will still be limited within a few Hertz [27]. Therefore, the application of SMA oscillators for vibration tuning can only be applied to those cases where the rate of change of the natural frequency of the primary system is rather slow (or even fixed), such as structure vibrations in civil engineering and some other application areas [6,28–37].

3. Modelling dynamics of shape memory alloys oscillators

For the analysis of the SMA oscillator for vibration tuning, it is essential to construct a suitable model for the SMA rod. It is self-evident that the model for this purpose has to be time-dependent since it is used in vibration tuning and loadings are dynamic. There have been developed many models to describe the behaviour of the SMAs, but most of them are only capable to capture static behaviour of the materials [17,38–40].

3.1. Dynamic models and their approximations

For the modelling of the response of SMAs under dynamic loadings, some additional issues need to be taken care of [41–43]. In order to make the dynamic problem trackable in engineering applications, a dimensional reduction of the fully coupled dynamic three-dimensional model for shape memory alloys was for the first time proposed in [44]. The reduced model was approximated by a system of differential–algebraic equations and was applied to the modelling of SMA-based devices such as actuators [45]. This approach allowed to study both stress- and temperature-induced phase transformations and associated hysteresis phenomena in SMA structures in a unified manner [46] and to extend the developed technique to the Cattaneo–Vernotte law for heat conduction following principles of extended thermodynamics in the context of SMA [15]. Multi-layered structures with embedded thermoelectric SMA actuators were considered as one of the areas of applications

of the developed dynamic models [47], and applications in nano-technology were discussed in [48,49]. The interest to shape memory effects in the context of the latter applications has been increasing and recently a number of materials that can have such effects under appropriate temperature conditions (e.g., Ni-based alloys) have been studied both theoretically [50] and experimentally [51].

In the multidimensional case, the developed approach for dynamic models of SMA and associated coupled multiscale problems [52,53] were put on a systematic basis via the centre-manifold theory and received its justification in a series of papers [54–56]. Two-dimensional thermo-mechanical waves in SMA patches were first analyzed in [57] and in [58] distributed mechanical loadings for patches of different sizes were studied. The results of such two-dimensional modelling were systematically compared with conventional one-dimensional models in [59], while in [60] the effectiveness of the developed procedure was demonstrated for both the solution of a transient uncoupled thermoelastic problem, for which an analytical solution is known, as well as for the fully coupled problem in the two-dimensional case. To make the dynamic model of SMA better amenable to engineering applications and to reduce further the computational cost, an empirical low dimensional model was developed based on a combination of proper orthogonal decomposition and Galerkin projection [61] which was applied to the modelling of martensitic phase transformations in ferroelectric/SMA patches [62]. Further analysis of such models was recently carried out in [63]. Another approach to dynamic models of SMA, based on the Chebyshev collocation method, was proposed in [64] where it was applied to the simulation of martensitic phase combinations in the 2D case. More recently, in [65] the dynamics of such combinations during thermally induced transformations was studied in detail. In [66], the developed methodology, based on Chebyshev's collocation, was applied to the analysis of SMA rods where the effect of internal friction was taken into account via Rayleigh's dissipation term. As expected, dissipation effects were enhanced by internal friction, while dispersion during wave propagations were induced by the presence of the interfacial energy term in the model. In [25] the method was applied to the analysis of macroscale damping effects induced by the first-order martensite phase transformations in a SMA rod. It was also shown that both mechanically and thermally induced phase transformations in SMA, as well as hysteresis effects, can efficiently be modelled by the finite volume method developed in [67] where it was applied in various one-dimensional (rods) and two-dimensional (patches) situations. A unified variational framework was applied to the analysis of SMA-based thin films [68] where phase nucleation under mechanical loading were reported. The approach combined the lattice-based kinetics involving the order variables and nonequilibrium thermodynamics [69]. The finite element based approach was extended to the three-dimensional situations and multivariant martensitic phase transformations [70,71], developed into a general framework [72], and exemplified with the analysis of cubic to tetragonal transformations [73]. Furthermore, a recently developed hybrid optimization methodology, combining the local and global search algorithms, has proved to be a useful tool in studying the dynamics of phase combinations in SMA samples [74]. A similar idea based on the genetic algorithm was recently pursuit in [75] specifically in the context of damping systems and seismic response mitigation.

From a practical point of view, the limitation of most prior analyses of the damping effects of SMAs have usually followed from approximations of constitutive laws based on separate phases, and the fact that the resulting strongly coupled nonlinear PDE models for SMA dynamics surveyed above are not easily amenable to control and the analysis of vibration tuning [41,21,9,10]. Recently, several important practical aspects of control for the above

problems, based on the feedback linearization, were discussed in [76,77].

3.2. Thermo-mechanical coupling and dissipation effects

In order to simulate the nonlinear restoring force in the SMA rod, in the context of our present problem, we start from a model that is able to capture the thermo-mechanical coupling effects and the first order phase transformations in the material. In particular, we employ the modified Ginzburg–Landau theory [20–22] where we deal with a two-way thermo-mechanical coupling: the mechanical oscillations induce temperature oscillations and the temperature changes in the material induce a mechanical response. In the present context, the temperature is considered to be a tool for the adjustment of material stiffness. As a result, we assume that it can be controlled (via heating or force air cooling) to a specific value for a specific vibration frequency and in what follows we focus on the description of the dynamics of the mechanical field.

To describe the dynamics of the mechanical field, we introduce the Lagrangian $\mathcal{L}$ of SMAs as the sum of kinetic and potential energy contributions:

$$\mathcal{L} = \int_0^L \left(\frac{\rho}{2} (\dot{u})^2 - \mathcal{F} \right) dx, \tag{3}$$

where ρ is the density of the material and u is the displacement in the SMA rod, $\mathcal{F}$ is the potential energy density of the material stored via deformations, while $\frac{\rho}{2}(\dot{u})^2$ models the kinetic energy density. An essential feature of the Ginzburg–Landau theory is that the potential energy density is a non-convex function of the chosen *order parameters* and temperature θ. We define this function as the sum of the local energy density ($\mathcal{F}_l$) and its non-local counterpart ($\mathcal{F}_g$). For the current one-dimensional problem, the strain $\varepsilon(x,t) = \frac{\partial u}{\partial x}$ is chosen as the order parameter, and the local free energy density can be constructed based on the Landau free energy density $\mathcal{F}_l(\theta, \varepsilon)$ [20,22]:

$$\mathcal{F}_l(\theta, \varepsilon) = \frac{k_1(\theta - \theta_1)}{2} \varepsilon^2 + \frac{k_2}{4} \varepsilon^4 + \frac{k_3}{6} \varepsilon^6, \tag{4}$$

where k_1, k_2, and k_3 are material-specific constants, θ_1 is the reference transformation temperature, which is also a material specific constant (to determine such parameters is often a non-trivial experimental task [78]). It has been shown that the above Landau free energy density is capable of modelling complicated thermo-mechanical coupling and hysteresis in the SMAs in the one dimensional description, as well as phase transformations in the material [20,22]. For different materials, the coefficients should be determined by fitting to experimental data.

The non-local free energy density is constructed in our case in a way similar to the free energy density for the class of ferroelastic materials as a function of the *order parameter* $\frac{\partial \varepsilon}{\partial x}$ [20]:

$$\mathcal{F}_g \left(\frac{\partial \varepsilon}{\partial x} \right) = k_g \left(\frac{\partial \varepsilon}{\partial x} \right)^2, \tag{5}$$

where k_g is a material-specific constant. The non-local term above accounts for inhomogeneous strain field. It represents energy contributions from domain walls of different phases. In order to account for dissipation effects, accompanying phase transformations, a Rayleigh dissipation term is introduced here as follows:

$$\mathcal{F}_R = \frac{1}{2} v \left(\frac{\partial \varepsilon}{\partial t} \right)^2, \tag{6}$$

where v is a material-specific constant. The dissipation term accounts for the internal friction accompanying the movement of the interfaces between different phases. At the macro-scale, it will

be translated into the viscous effects of phase transformations [20,18].

By substituting the potential energy density into the Lagrangian function given by Eq. (3) and setting the variation of the functional with respect to the variation of $u(x, t)$ (the true path) to zero according to the Hamilton's principle, one has:

$$\delta \int_0^T \mathcal{L} dt = \int_0^T \int_0^L \delta \left(\frac{\rho}{2} (\dot{u})^2 - \mathcal{F} \right) dx dt = 0. \tag{7}$$

The governing equation for the dynamics of the mechanical field, taking into account dissipation effects, has the form:

$$\rho \ddot{u} = \frac{\partial}{\partial x} \left(k_1(\theta - \theta_1)\varepsilon + k_2 \varepsilon^3 + k_3 \varepsilon^5 \right) + v \frac{\partial}{\partial t} \frac{\partial^2 u}{\partial x^2} - k_g \frac{\partial^4 u}{\partial x^4}. \tag{8}$$

This is re-cast in the form of the following system of differential–algebraic equations:

$$\begin{aligned} \rho \ddot{u} &= \frac{\partial \sigma}{\partial x} + v \frac{\partial}{\partial t} \frac{\partial^2 u}{\partial x^2} - k_g \frac{\partial^4 u}{\partial x^4}, \\ \sigma &= k_1(\theta - \theta_1)\varepsilon + k_2 \varepsilon^3 + k_3 \varepsilon^5, \end{aligned} \tag{9}$$

supplemented by boundary conditions for stress σ: $\sigma(0) = \sigma_L$, $\sigma(L) = \sigma_R$ with given values of σ_L and σ_R where L is the length of the SMA rod.

When the thermal field of the coupled thermo-mechanical dynamics of the SMA has to be accounted for, the governing equation for the temperature can be formulated by employing the conservation law of internal energy:

$$\rho \frac{\partial e}{\partial t} + \frac{\partial q}{\partial x} - \sigma \frac{\partial \varepsilon}{\partial t} - v \frac{\partial \varepsilon}{\partial t} \frac{\partial \varepsilon}{\partial t} - k_g \frac{\partial^2 \varepsilon}{\partial x \partial t} = 0, \tag{10}$$

where e is the internal energy, $q = -k \partial \theta / \partial x$ is the (Fourier) heat flux, k is the heat conductance coefficient of the material.

For formulating the governing equation in terms of temperature, the internal energy is associated with the non-convex potential energy mentioned above via the Helmholtz free energy function as follows:

$$\mathcal{H}(\theta, \varepsilon) = \mathcal{F}_l(\theta, \epsilon) - c_v \theta \ln \theta \tag{11}$$

where c_v is the specific heat capacitance. The thermodynamic equilibrium condition gives:

$$e = \mathcal{H} - \theta \frac{\partial \mathcal{H}}{\partial \theta}, \quad \sigma = \frac{\partial H}{\partial \varepsilon}. \tag{12}$$

By substituting the above relationships into Eq. (10), the governing equation for the thermal field can finally be formulated as follows:

$$c_v \frac{\partial \theta}{\partial t} = k \frac{\partial^2 \theta}{\partial x^2} + k_1 \theta \varepsilon \frac{\partial \varepsilon}{\partial t} + v \left(\frac{\partial \varepsilon}{\partial t} \right)^2. \tag{13}$$

Since the SMA oscillator considered here is used as an adaptive vibration absorber via adjusting its temperature, the temperature is assumed to be completely controlled by external inputs. This results in a situation where there is no need for the simulation of temperature field evolution and the main focus in the analysis that follows will be given to the mechanical field, although the thermo-mechanical coupling will still be accounted for, e.g. through the restoring force.

3.3. Nonlinear simplified model

The dependency of the dynamics of the mechanical field on the temperature is included in the above formulation. Recently we demonstrated that this model is able to capture the thermo-mechanical coupling effects and the first order phase transformations in SMA rods [22]. However, the main difficulty in applying

the above model to the analysis of vibration tuning in the context of our present problem is that the dynamic response simulation (accompanied by the simulation of phase transformations and wave propagations in the SMA rod) is computationally too costly for most engineering problems. We note that for our current problem, phase transformations and wave propagations in the SMA rod (on the order of sound speed) are taking place much faster compared to the vibration speed of the mass blocks. Therefore, in the first approximation we only consider the steady counterpart of Eq. (9). With the above observation in mind, we set all time derivative terms in Eq. (9) to zero which leads to the following simplified model:

$$\sigma = k_1(\theta - \theta_1)\varepsilon + k_2\varepsilon^3 + k_3\varepsilon^5, \quad \sigma(0) = \sigma_L, \ \sigma(L) = \sigma_R. \tag{14}$$

where the inhomogeneous strain term is also ignored, since the stress in solid structures will be uniform when it is at equilibrium states under boundary loadings, provided that there is no body force. The same applies to the strain in the structure. By using the above argument, the strain distribution in the SMA rod can be calculated as $\varepsilon = \Delta L/L$. The mass of the SMA rod is effectively ignored due to the fact that it is much smaller compared to the mass block m_a. In this case, the force–deformation relation for the SMA rod can be obtained in the following form:

$$F_s = \beta\left(k_1(\theta - \theta_1)\frac{\Delta L}{L} + k_2\left(\frac{\Delta L}{L}\right)^3 + k_3\left(\frac{\Delta L}{L}\right)^5\right), \tag{15}$$

where β is the cross-sectional area of the SMA rod and ΔL is the deformation due to force. By choosing appropriate β and L values, and assuming that one end of the SMA rod is fixed on the primary mass block while the other is on the attached block, we are able to formulate the restoring force as follows:

$$F_s = K_1\Delta\theta(x_p - x_a) + K_2(x_p - x_a)^3 + K_3(x_p - x_a)^5, \tag{16}$$

where the definition of K_1, K_2 and K_3 is obvious from the above equation, and $(\theta - \theta_1)$ in the previous equations is replaced by $\Delta\theta$.

The restoring force is shown to be dependent on the temperature, due to the thermo-mechanical coupling effects.

If the internal viscosity of the SMA rod is also taken into account, then the term $\nu\frac{\partial}{\partial t}\frac{\partial^2 u}{\partial x^2}$ in Eq. (8) should not be set to zero (see [44,54] for the original general model of this type and its low dimensional reductions) because F_s will not be a pure elastic force, but rather a combination of the following forces:

$$F_s = K_1\Delta\theta(x_p - x_a) + K_2(x_p - x_a)^3 + K_3(x_p - x_a)^5 + c_v(\dot{x}_p - \dot{x}_a). \tag{17}$$

Here, the contribution of the friction force $c_v(\dot{x}_p - \dot{x}_a)$ plays a similar role to the term $c_p\dot{x}_p$ in the primary system. For the illustration of frequency adjustability, the friction force of the SMA oscillator is neglected in computational experiments reported in Section 4.

The model for the SMA rod given by Eq. (16) is nonlinear. For the convenience of analysis, we introduce an equivalent stiffness K_e for the SMA rod, which leads to the following difference squared being minimized:

$$\int_{x_b}^{x_t} (F_s(x_p - x_a) - F_a(x_p - x_a))^2 dx, \tag{18}$$

where $F_s(x_p - x_a)$ is the restoring force calculated by using Eq. (16) and $F_a(x_p - x_a) = K_e(x_p - x_a)$ is the linear approximation that is calculated by using the equivalent stiffness. Values x_b and x_t are the minimal and maximal values for $x_p - x_a$, which is chosen before the simulation. Finally note that the estimated K_e also depends on the choice of x_b and x_t.

To illustrate the dependence of the equivalent stiffness of the SMA rod on temperature, the force–deformation relations given by Eq. (16) are plotted for the material $Au_{23}Cu_{30}Zn_{47}$ with four

different temperatures in Fig. 2 (solid curves), together with those obtained with estimated equivalent stiffness (dashed straight lines). The SMA rod length is chosen 4 m with cross-section area being $\beta = 3.83 \times 10^{-5}$ m^2. The details of all other parameters for this material are given in Table 1 (see Ref. [13,46,79]). The hysteresis is observed when $\theta = 210$ K, as indicated by the dashed lines with arrows in the sub-plot (a). It is worth also to note that the force–deformation relation given by Eq. (16) cannot be linearized, in particular for the low temperature case, because it does not correspond to a stable structure. In the high temperature case, the behaviour of the SMA rod is very close to the behaviour of a linear spring, but with its stiffness linearly dependent on its temperature.

It can be further demonstrated that the nonlinear restoring force given by Eq. (16) can be regarded as a general model for the behaviour of SMA rods with nonlinear thermo-mechanical coupling and hysteresis induced by phase transformations. One can associate the following potential energy with nonlinear restoring force:

$$\Psi = \frac{K_1}{2}\Delta\theta(x_p - x_a)^2 + \frac{K_2}{4}(x_p - x_a)^4 + \frac{K_3}{6}(x_p - x_a)^6. \tag{19}$$

Without loss of generality, the parameter values for K_1, K_2 and K_3 can be calculated by using the vlaues for k_1, k_2 and k_3 as given in Table 1, and the phase transformations can qualitatively be analyzed by studying system equilibria and "switches" indicated by the energy profiles [15] (focusing on the profiles themselves, the associated energy units of Ψ are not essential). Three different profiles of Ψ with three different temperatures are plotted in Fig. 3.

Analyzing the subplot (a), we conclude that at low temperature ($\theta = 210$ K), there are two equilibria which are energetically equivalent. The system state can be switched from one of the equilibria to another provided that the external loading exceeds a certain value and overcomes the energy barrier. This switching will induce hysteresis, as indicated by the associated constitutive curve plotted in Fig. 2 (a). At the same time, the switching also dissipates the input energy. At high temperature ($\theta = 320$ K), as plotted in the subplot (c), the potential energy has a single equilibrium, and there is no state switching in the system dynamics, but the thermomechanical coupling still exists. In this case, the SMA behaves more like an elastic material, except that its stiffness depends on its temperature. When the materials temperature is intermediate ($\theta = 245$ K), the potential energy has two local equilibria (far from the centre) and one global equilibrium (at the centre), as plotted in the subplot (b). Under external loadings, there are still system state switchings from one equilibrium to another, which indicates that hysteresis loops will be induced. However, the energy barrier between the centre equilibrium and the two local equilibria are smaller than those at low temperatures, which means that the system state can be switched more easily, and hysteresis loops will have smaller enclosed areas. The energy dissipation is also less. Due to continuous dependency of the potential energy on the temperature, the transition of the potential energy from low temperature to high temperature profiles will also be continuous, as well as the corresponding constitutive laws, as indicated in Fig. 2. A detailed analysis of phase transformations according to the potential energy profiles was given in Ref. [20] and developed further and applied in a number of papers (see [15,66] and references therein).

Before moving to the discussion of numerical results, we note that the three coefficients k_1, k_2, and k_3 in Eq. (10) are given, once the SMA material is chosen (these are materials constants). Moreover, at a specified temperature, the force–deformation relation of the SMA rod is well defined based on such three constants, as illustrated by Fig. 2. We refer the interested reader to further discussions on the physical interpretation of these three materials constants in [13,20,80,46]. Finally, we recall that the three coefficients K_1, K_2, and K_3 in Eq. (12) are directly related to k_1, k_2, and
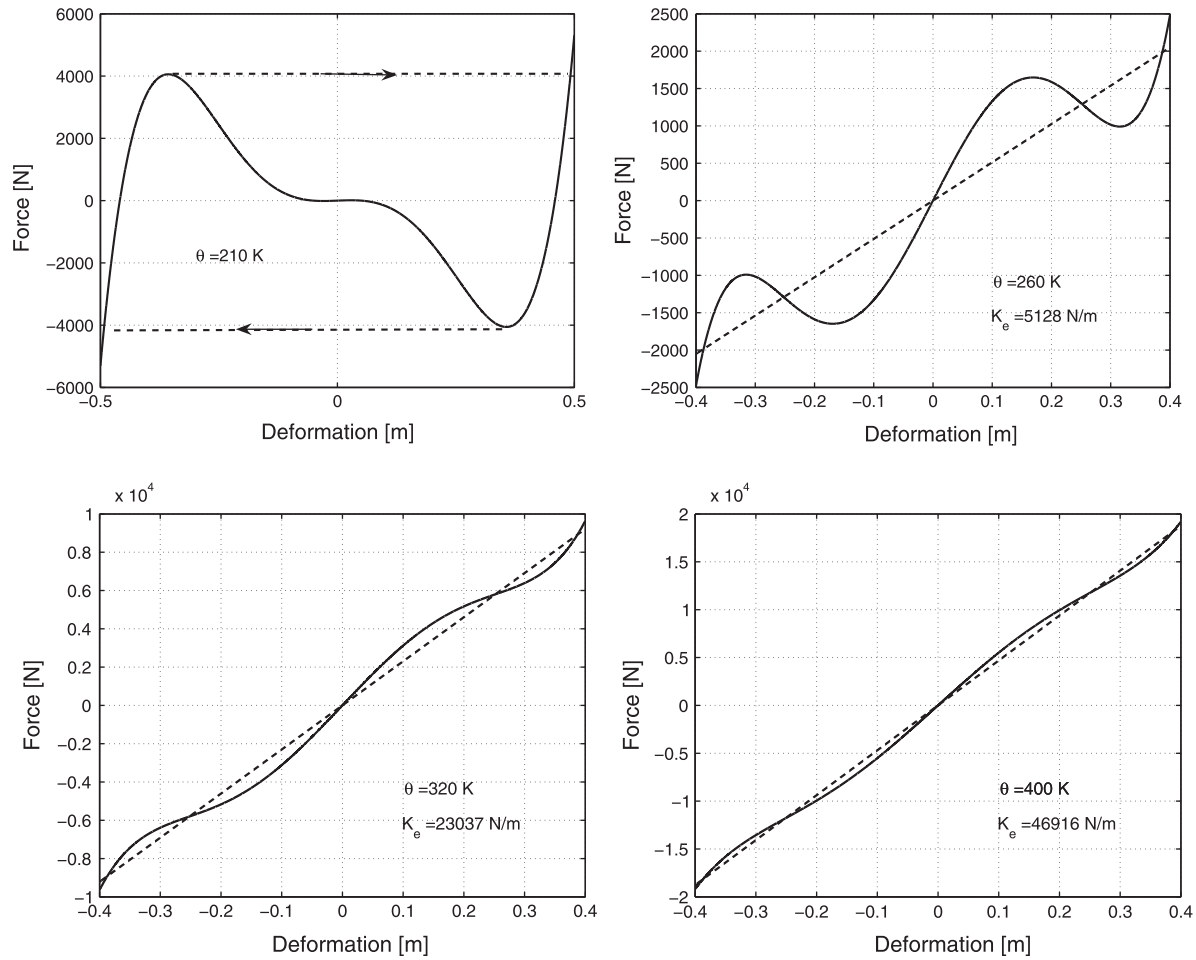
Fig. 2. Sketch of force–deformation relations of a shape memory alloy rod. From left to right, top to bottom, (a) θ = 210 K, (b) θ = 260 K, (c) θ = 320 K, and (d) θ = 400 K.

Table 1
Parameters of the shape memory alloy vibration absorber.

Parameter	Value (unit)	Parameter	Value (unit)
m_p	10 kg	k_p	64,000 N/m
m_a	5 kg	c_p	100 Ns/m
t_0	0 s	t_f	10 s
θ_0	208 K	k_1	4.8×10^7 kg/s^2 mK
k_2	6.0×10^{11} kg/s^2 m	k_3	8.0×10^{13} kg/s^2 m
β	3.83×10^{-5} m^2	L	4 m

k_3 and their actual values depend also on the values of β and L for a specific SMA sample.

We also note that, depending on the application at hand, the primary system may be vibrating with unknown multiple frequencies or with a drifting mono-frequency, and both of these situations should be accounted for in the actual design of supplementary oscillators. Let us consider these situations in further detail.

When the primary system is vibrating with unknown multiple frequencies, supplementary oscillators normally will not perform well by tuning their own natural frequencies in this case, because one supplementary oscillator can absorb only the vibration energy of a single frequency component which matches with the supplementary oscillator, with no effects (or very minor effects) on other frequency components. When the SMA oscillator is used in this case, it could be tuned to work in its low temperature range in which the martensite transformations could be induced. However,

such martensite transformations and martensite re-orientations are always accompanied by mechanical energy dissipation, and as a result, a broad-band vibration attenuation might be induced. In this case, the mechanism of vibration suppression will be different from that of attaching supplementary oscillators. The interested reader is referred to [25] for further discussion on vibration damping by using the mechanically induced phase transformations in SMAs in a situation described above.

When the primary system is vibrating with a drifting mono-frequency, the supplementary SMA oscillator should be tuned to work in its high temperature range, in which no phase transformations are expected. In this case, the restoring force can be approximated very well by using an equivalent stiffness calculated by Eq. (14), and the natural frequency of the SMA oscillator is adjustable via changing its temperature. For practical design, the equivalent stiffness can be obtained via function approximation methods as follows. For example, in Eq. (14), the equivalent stiffness K_e is estimated in such a way that $F_a(x_p - x_a) = K_e(x_p - x_a)$ is the best approximation to the nonlinear restoring force given by Eq. (12), in the sense of least square error. Therefore, the approximation error function should be orthogonal to $(x_p - x_a)$ which implies that:

$$\langle F_s(x_p - x_a) - K_e(x_p - x_a), (x_p - x_a) \rangle = 0, \tag{20}$$

where $\langle , \rangle$ is the inner product of two functions on the specified domain. The latter immediately leads to the following result for the estimated stiffness K_e:

$$K_e = \frac{\langle F_s(x_p - x_a), (x_p - x_a) \rangle}{\|x_p - x_a\|}. \tag{21}$$
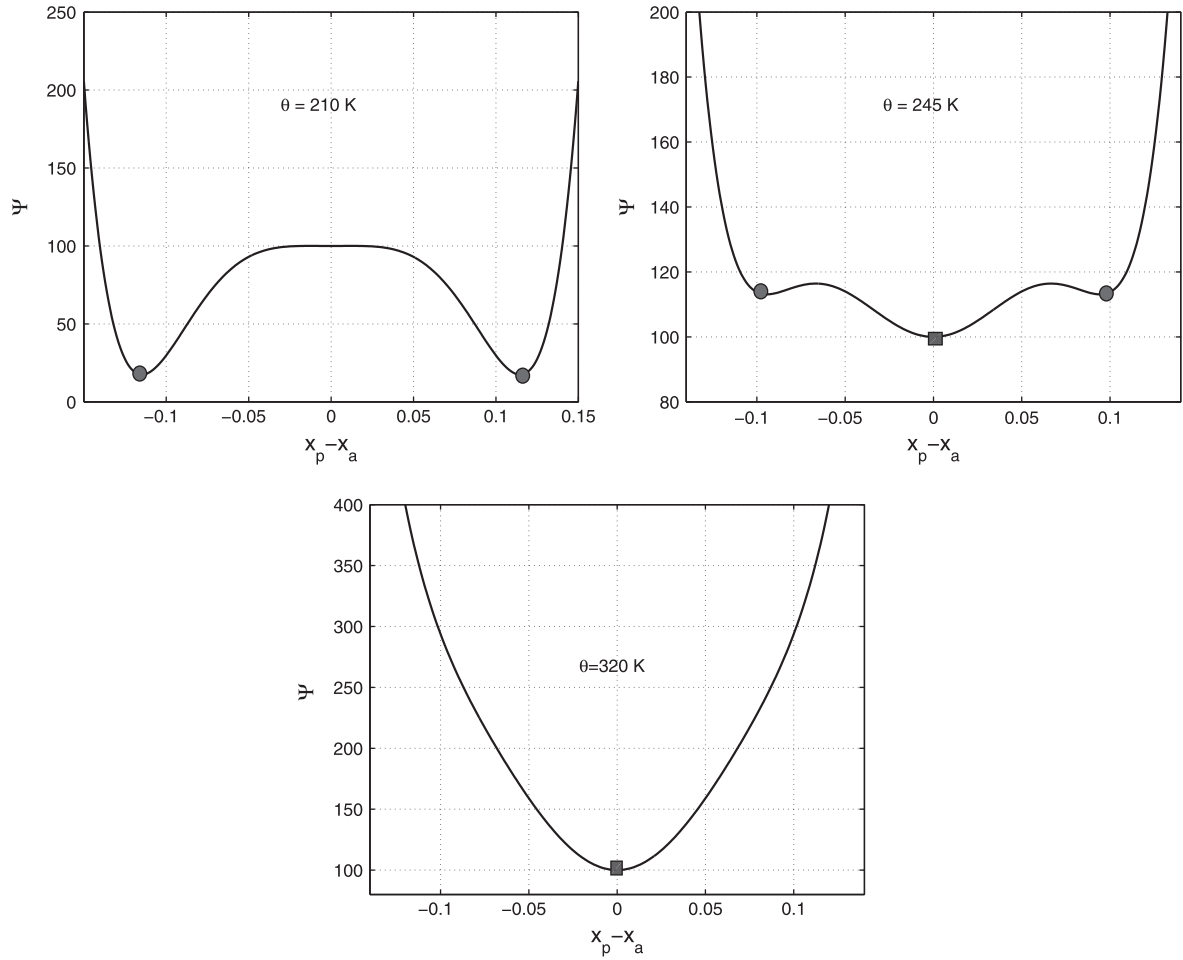
Fig. 3. Sketch of potential energy of a shape memory alloy rod at different temperatures. From left to right, top to bottom, (a) θ = 210 K, (b) θ = 245 K, and (c) θ = 320 K.

Note that since F_s depends on the material temperature, the estimated equivalent stiffness will be dependent on the temperature too. If there is no phase transformations induced in the SMA oscillator, the equivalent stiffness can be treated as a linear function of the material temperature:

$$K_e = \frac{\langle K_1 \Delta\theta(x_p - x_a) + K_2(x_p - x_a)^3 + K_3(x_p - x_a)^5, (x_p - x_a)\rangle}{\|x_p - x_a\|}$$
$$= K_1\Delta\theta + \frac{\langle K_2(x_p - x_a)^3 + K_3(x_p - x_a)^5, (x_p - x_a)\rangle}{\|x_p - x_a\|}. \quad (22)$$

In practical design of supplementary oscillators, it is often reasonable to attempt to tune the SMA oscillator to work in its high temperature range, based on a specified frequency range within which the vibration frequency of the primary system is drifting (given some restrictions on the range of the frequency drifting). What is important is that once the SMA material is chosen, and the highest and lowest vibration frequencies of the primary system are specified, we can choose different β and L values to tune the parameters K_1, K_2 and K_3 in such a way that the estimated equivalent stiffness (determined by Eq. (22)) matches with the specified frequency range, by changing the material temperature and avoiding the martensite phase transformation at the same time. It should be noted that the estimated equivalent stiffness in Eq. (22) also depends on the displacement $(x_p - x_a)$ of the secondary system, which is often empirical for the oscillator design. However, if one use the K_e estimated with an empirically specified $(x_p - x_a)$ to determine the material temperature according to Eq. (22) in matching the natural frequency of the oscillator with the drifting

frequency of the primary system, then the SMA oscillator will not perform well because the simulated $(x_p - x_a)$ will likely be different from the specified one. In order to get the right material temperature for the frequency match, one needs to iterate with updated $(x_p - x_a)$ values for a few cycles.

Our last comment in this section is related to the fact that in most practical designs the SMA oscillator does not work alone. Indeed, it often works with an elastic spring in parallel which leads to a situation where the restoring force given in Eq. (12) can be easily adjusted according to the structure design. For example, when the SMA oscillator works with a spring in parallel and the stiffness of the spring is K_s, then the total restoring force of the SMA rod and the elastic spring is given by:

$$F_s = K_1\Delta\theta(x_p - x_a) + K_2(x_p - x_a)^3 + K_3(x_p - x_a)^5 + K_s(x_p - x_a)$$
$$= (K_s + K_1\Delta\theta)(x_p - x_a) + K_2(x_p - x_a)^3 + K_3(x_p - x_a)^5. \quad (23)$$

The above clearly shows that by using a spring in parallel with the SMA oscillator we are achieving the result equivalent to adjusting one of the coefficients in the nonlinear restoring force. By combining the above equation with Eq. (22), the following equivalent stiffness estimation can be obtained:

$$K_e = \frac{\langle (K_1\Delta\theta + K_s)(x_p - x_a) + K_2(x_p - x_a)^3 + K_3(x_p - x_a)^5, (x_p - x_a)\rangle}{\|x_p - x_a\|}$$
$$= K_s + K_1\Delta\theta + \frac{\langle K_2(x_p - x_a)^3 + K_3(x_p - x_a)^5, (x_p - x_a)\rangle}{\|x_p - x_a\|}. \quad (24)$$

Hence, the spring in parallel with the SMA oscillator can be regarded as another degree of freedom in tuning the equivalent stiffness of the vibration absorber. A similar analysis can be carried out for a series of springs used with SMA oscillators, connected with each other.

4. Numerical results and discussions

### 4.1. Material parameters and validations

Experimental measurements on damping properties of shape memory alloys are becoming more readily available. For example, in [81] the authors investigated both elastic and damping properties of Cu–Al–Ni single crystal shape memory alloys for several frequencies of the oscillating force. Such results, in particular for the evolution of damping in cooling/heating measurements can give information about internal friction during forward and reverse martensitic phase transformations. Nevertheless, results on damping properties of shape memory alloy materials are still sketchy in the literature. In what follows we will show a proof of concept for the feasibility of frequency tuning in shape memory alloys based on the model developed in the previous section. All details of the parameters used in our examples discussed below are given, providing the scope for further analysis of the proposed concept and comparisons. In addition to single Cu–Al–Ni crystals mentioned above, experimental data on some other single crystals, such as $Au_{23}Cu_{30}Zn_{47}$ and

CuZnAl, is also available in the literature. To be specific, we based our analysis on $Au_{23}Cu_{30}Zn_{47}$ as this specific SMA material has been attracting attention of many researchers since the fundamental paper by Falk [13] where the interested reader can find both the original model and relevant parameters are both given and where the comparison with experimental results was also given. Since then this material and its parameters have been used in a number of works on the analysis of SMA properties (e.g., [79,46]. For CuZnAl single crystals, this Falk model based Ginzburg–Laudan theory was also analyzed and comparisons of the results with those experimentally obtained were reported showing good agreement [80,82,83]. Based on the same validated model, we derived a simple and efficient model easily amenable to practical applications.

The numerical experiments presented here have been carried out for a SMA oscillator designed for vibration suppression of engineering structures (such as buildings which are excited externally in the horizontal direction and whose bases could be regarded as a visco-elastic connection, as sketched in Fig. 1, left. The system can be interpreted through the vibration of the two mass blocks sketched in Fig. 1, (right).

4.2. Temperature adjustments

Using Eq. (16) for the nonlinear restoring force of the SMA oscillator, the governing equation for the primary and attached system can be formulated finally as follows:
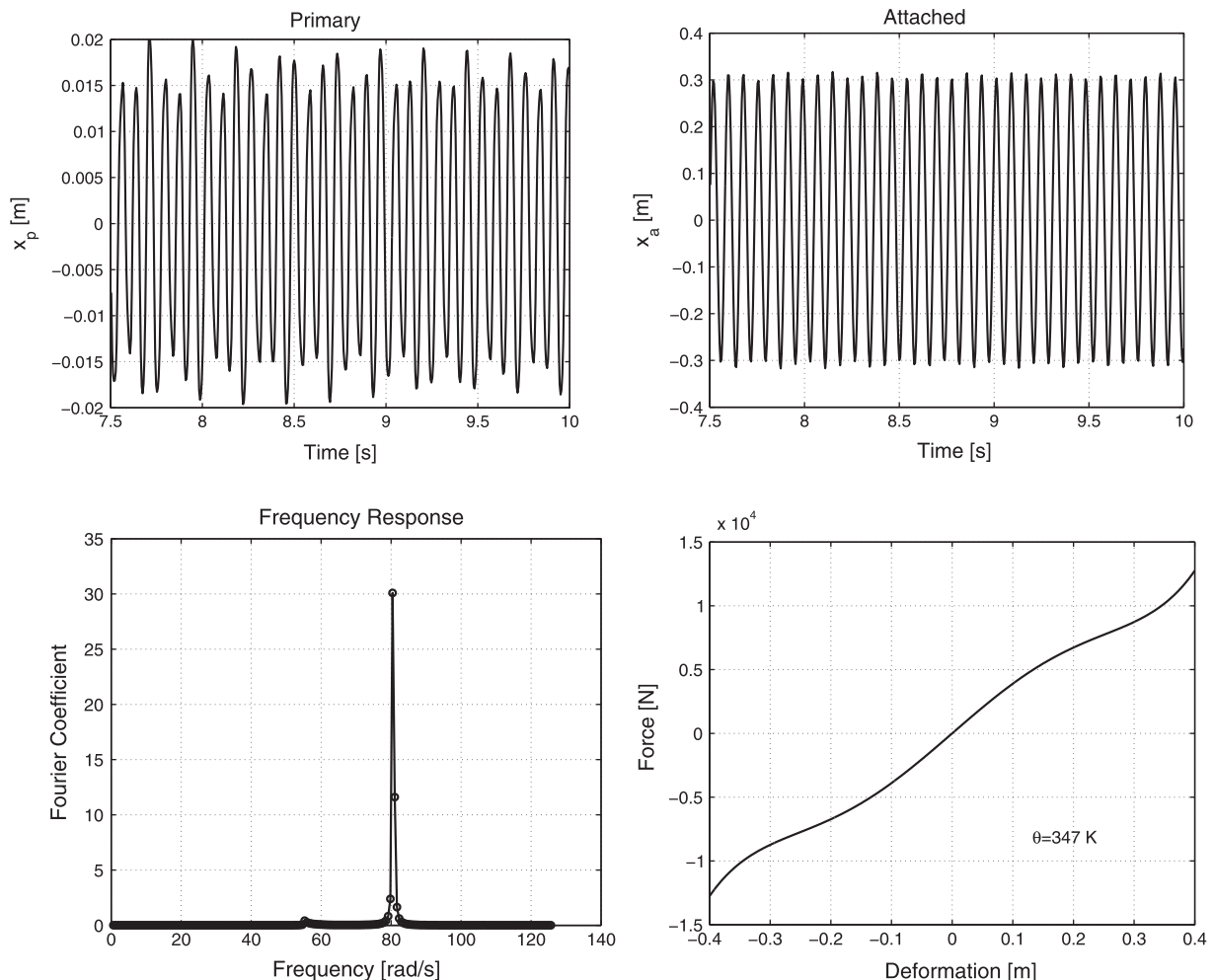
Fig. 4. Numerical simulation of the vibration absorption using a shape memory alloy oscillator. From left to right, top to bottom, (a) displacement of the primary mass block, (b) displacement of the attached mass block, (c) frequency response of the absorber, (d) force–deformation relation of the absorber.

$$m_p\ddot{x}_p + c_p\dot{x}_p + k_px_p + K_1\Delta\theta(x_p - x_a) + K_2(x_p - x_a)^3 + K_3(x_p - x_a)^5 = F(t),$$
$$m_a\ddot{x}_a = K_1\Delta\theta(x_p - x_a) + K_2(x_p - x_a)^3 + K_3(x_p - x_a)^5.$$

$$(25)$$

By applying these equations, the vibration of the primary and at-tached blocks can be simulated simultaneously and, as a result, their velocities can be obtained. The parameters for the numerical simulation are listed in Table 1, from which the natural frequency of the primary system can be calculated as $\omega_n = \sqrt{k_p/m_p} = 80$ rad/s.

For illustration purposes, we first employ an excitation force with mono-frequency equal to the natural frequency of the primary system:

$$F(t) = 1.0 \times 10^4 \sin(\omega_n t). \tag{26}$$

There will be a resonance induced if there is no vibration absorber attached to the system. Ideally, if ω_n is already known, a linear oscillator can be designed to completely suppress the vibrations of the primary mass. However, if ω_n is unknown or drifting, one has to employ an adaptive vibration absorber. As indicated in Ref. [8], the performance of adaptive vibration absorbers are not as good as idealized linear oscillators for vibrations with a speci-fied frequency, and the vibrations of the primary block might not be able to be suppressed completely [8]. In our representative computational experiment reported below, we employ a SMA ab-sorber for vibration tuning with parameters of the absorber listed in Table 1 and its temperature chosen at $\theta = 347$ K.

The simulation results with this temperature for the vibration absorption are presented in Fig. 4. The displacement x_p and x_a are only plotted for the last one fourth of the entire simulated interval, which is [7.5, 10]s, in sub-plots (a) and (b), respectively. These re-sults demonstrate that the attached block has a much larger ampli-tude compared to that of the primary block. In its turn, this indicates that most of vibration energy is absorbed by the attached oscillator. The vibration amplitude of the primary block is around 0.02 m, which is less than one tenth of that of the attached block. A discrete Fourier transformation is performed on the simulated displacement of the SMA oscillator, and its spectrum is presented in the sub-plot (c). This result indicates that the response of the SMA oscillator with the current temperature can be approximated very well by a linear oscillator because it has the same frequency response as linear oscillators have. Furthermore, the constitutive relation that accounts for the force–deformation relation of the SMA rod is plotted in the sub-plot (d). It also implies a linear-like relation.

Note that the way we have used to estimate the temperature for the SMA absorber for a given excitation frequency is based on the equivalent stiffness of the SMA rod. Calculations according to Eq. (18) indicate that for $\theta = 350$ K the SMA rod will have an equivalent stiffness 3.2×10^4 which gives a natural frequency 80 rad/s. Since
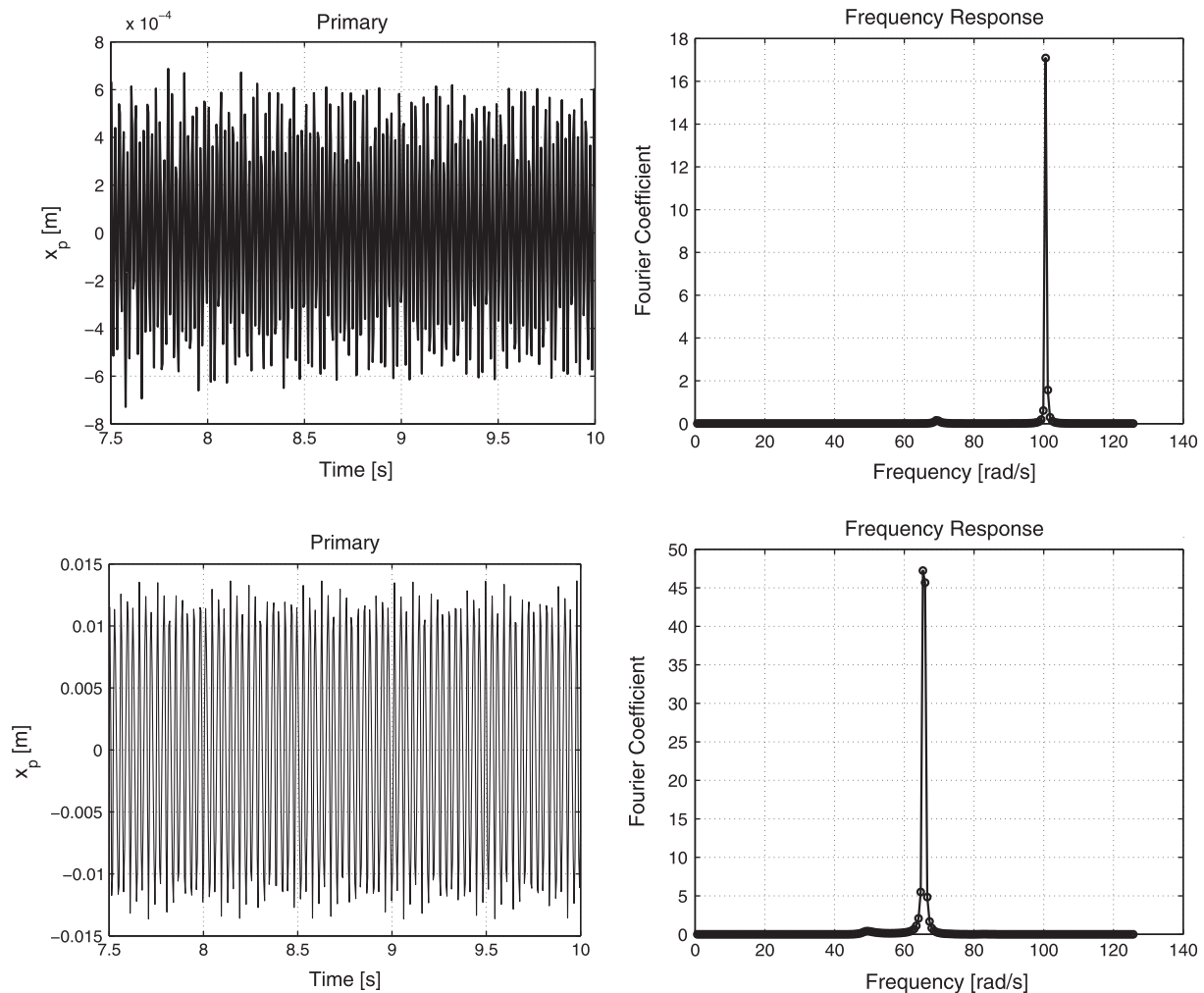
Fig. 5. Numerical simulation of the adaptivity of SMA vibration absorber. From left to right, top to bottom, (a) displacement of the primary mass, $\theta = 396$ K. (b) Frequency response of the absorber, $\theta = 396$ K. (c) Displacement of the primary mass, $\theta = 282$ K. (d) Frequency response of the absorber, $\theta = 282$ K.

the system is nonlinear, the estimated equivalent stiffness depends on the chosen deformation range which is influenced by other parameters like m_a, etc. Therefore, for a better performance, the temperature of the SMA absorber should be slightly adjusted around the estimated temperature according to the equivalent stiffness. Indeed, several iterations carried out with the developed numerical procedure brings us to a more refined temperature value of $\theta = 347$ K.

4.3. Adaptivity

To demonstrate the operation of the SMA oscillator as an adaptive vibration absorber, the stiffness of the spring in the primary system is now changed to $k_p = 100^2 \, m_p$, so its natural frequency becomes 100 rad/s, and the frequency of the excitation is changed to 100 rad/s as well. For the vibration absorbing using the SMA oscillator, its temperature is estimated around $\theta = 403$ K, at which level its equivalent stiffness is $K_e = 5 \times 10^4$ N/m. This yields a natural frequency 100 rad/s for the SMA oscillator. Once again, a few iterations lead us to a more refined temperature value of $\theta = 396$ K. The displacement of the primary mass is sketched in a similar way as before in part (a) of Fig. 5, and the frequency response of the absorber is plotted in part (b). It is shown that the vibration

amplitude is very small, indicating that the performance of the absorber is very good at this temperature. This can be explained by the fact that the SMA behaviour is similar to the behaviour of a linear spring at high temperatures, which is also demonstrated by the frequency response plot.

Next, the frequency of the primary system and excitation is changed to 65 rad/s, and all other conditions are kept unchanged. For this case, the temperature of the SMA absorber is estimated to be $\theta = 282$ K. Results of numerical simulations for this case are shown in Fig. 5, in part (c) and (d) for x_p and frequency response, respectively. This result indicates that the amplitude of x_p is still successfully reduced to a very small value, and the behaviour of the absorber is still similar to linear absorbers.

In the above numerical simulations, the SMA oscillator was working at high temperatures, corresponding to the situations where the SMA rod was in the austenite phase and no hysteresis effects were observed. To exploit the application potential of the hysteresis due to phase transformations in the SMA rod, we simulate the operation of the oscillator for in the low temperature case by setting $\theta = 210$ K. Due to non-convexity of the force–deformation relation under this temperature (see Fig. 2, part (a)), it is not reasonable to attempt estimating the equivalent stiffness as we did before. Our purpose now is to demonstrate a general vibration
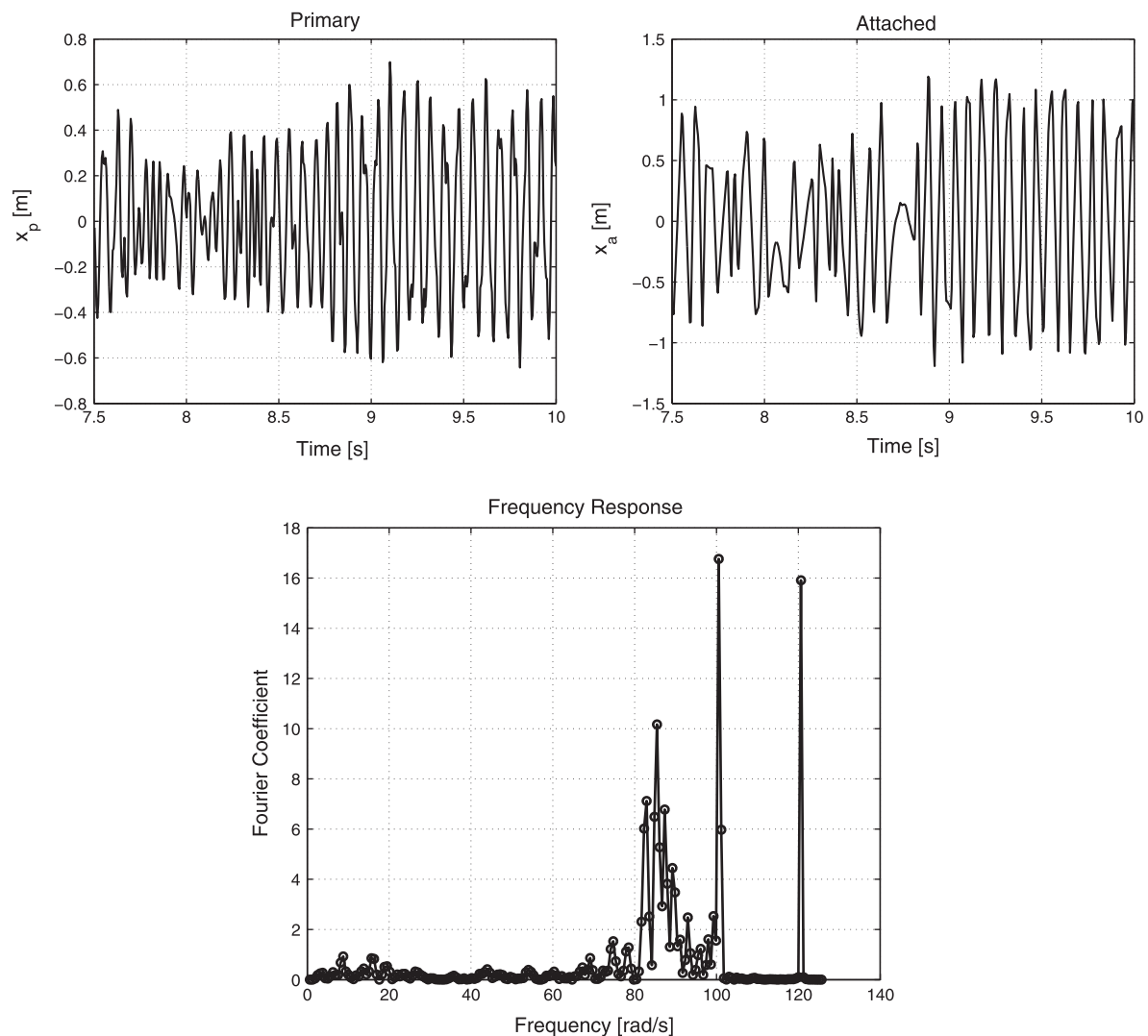
Fig. 6. Numerical simulation of the vibration absorption using a shape memory alloy oscillator. From left to right, top to bottom, (a) displacement of the primary mass; (b) displacement of the attached mass; (c) frequency response of the absorber.

attenuation trend of the SMA oscillator at low temperature. The friction force in the primary system is set to zero in this experiment ($c_p = 0$), and frequency is adjusted to $\omega_n = 120$ rad/s by changing k_p accordingly. The excitation varies according to the following switching function:

$$F(t) = 1.0 \times 10^4 \text{sign}(\sin(\omega_n t)), \qquad (27)$$

where the function sign ($\cdot$) has value 1 if the variable is positive and value -1 when it is negative. The results of numerical simulations are shown in Fig. 6.

The amplitude of x_p and x_a show that the major part of the energy is absorbed by the oscillator because the latter has a larger amplitude. If the temperature is sustained at low values, the vibration energy in the SMA oscillator will be dissipated continuously to make the vibration of the primary system attenuated [9,12]. However, the amplitude of x_p is much larger compared to those values obtained in the above simulations. These observations indicate that although the performance of the SMA absorber in the low temperature regime is not very satisfactory, they show its robustness, in particular in those cases when the excitation does not exhibit a harmonic pattern and is not a priori known. The frequency response is much more complicated in this case due to the fact that nonlinearities in the force–deformation relation become dominant at this temperature, precluding us from linear spring type approximations.

Based on estimated values of temperature for the vibration absorption, the above results have demonstrated that the vibrations of the primary mass block are successfully attenuated by using the SMA absorber. In the general case, due to nonlinearity of the force–deformation relation, the best temperature for the vibration absorption should be found by using an appropriate optimization procedure.

5. Conclusions

In this paper, we proposed a dynamic nonlinear model for SMA-based oscillators in the vibration absorption applications and evaluated the performance of such oscillators. An essential part of such oscillators – the SMA rod – was modelled on the basis of the Ginzburg–Landau theory. The resulting nonlinear model accounted for both thermo-mechanical coupling and hysteresis effects induced by phase transformations. Numerical simulations, carried out for various excitation frequencies, demonstrated that the SMA vibration absorber could be adaptive in a sense that it could be adjusted to match different frequencies by changing its temperature. Recently, practical aspects of control of shape memory alloy materials, based on the feedback linearization, were discussed in [76,77]. Finally we note that in this contribution, it was demonstrated that the SMA absorber could be used as a general vibration attenuator in low temperature regimes, with robust features observed in the situations where the frequency information about the primary system and excitation is a priori unknown.

References

[1] Harris CM. Shock and vibration handbook. New York: McGraw-Hill; 1996.
[2] Ogata K. System dynamics. New York: Pearson Education; 2004.
[3] McGavin G, Guerin G. Real-time seismic damping and frequency control of steel structures using Nitinol wire. Proc SPIE 2002;4696:176–84.
[4] Heinonen J, Vessonen I. Controlling stiffness of a frame spring by changing the boundary condition with an SMA actuator. Comput Struct 2008;86(3–5):398–406.
[5] Hashemia SMT, Khademb SE. Modeling and analysis of the vibration behavior of a shape memory alloy beam. Int J Mech Sci 2006;48:44–52.
[6] Song G, Ma N, Li NH. Applications of shape memory alloys in civil structures. Eng Struct 2006;28(9):1266–74.
[7] Williams KA, Chiu GTC, Bernhard RJ. Passive adaptive vibration absorbers using shape memory alloys. Proc SPIE 1999;3668:630–41.
[8] Williams KA, Chiu GTC, Bernhard RJ. Dynamic modelling of a shape memory alloy adaptive tuned vibration absorber. J Sound Vib 2005;280:211–34.
[9] Masuda A, Noori M. Optimisation of hysteretic characteristics of damping devices based on pseudoelastic shape memory alloys. Int J Nonlinear Mech 2002;37:1375–86.
[10] Piedboeuf MC, Gauvin R, Thomas M. Damping behaviour of shape memory alloys: Strain amplitude, frequency and temperature effects. J Sound Vib 1998;214(5):885–901.
[11] Rustighi E, Brennan MJ, Mace BR. A shape memory alloy adaptive tuned vibration absorber: design and implementation. Smart Mater Struct 2005;14:19–28.
[12] Saadat S, Salichs J, Noori M, Hou Z, Davoodi H, Bar-on I, et al. An overview of vibration and seismic applications of NiTi shape memory alloy. Smart Mater Struct 2002;11:218–29.
[13] Falk F. Model free energy, mechanics, and thermomechanics of shape memory alloys. Acta Metall 1980;28:1773–80.
[14] Peultier B, Benzineb T, Patoor E. Modelling of martensitic phase transformation for finite element computation. J Phys IV France 2004;115:351–9.
[15] Melnik RVN, Roberts AJ, Thomas KA. Phase transitions in shape memory alloys with hyperbolic heat conduction and differential–algebraic models. Comput Mech 2002;29(1):16–26.
[16] Pieczyska E, Gadaj S, Nowacki WK, et al. Characteristics of energy storage and dissipation in TiNi shape memory alloy. Sci Technol Adv Mater 2005;6(8):889–94.
[17] Auricchio F, Sacco E. Thermomechanical modelling of a superelasitc shape memory wire under cyclic streching–bending loadings. Int J Solid Struct 2001;143:175–94.
[18] Sun S, Rajapakse RKND. Simulation of pseudoelastic behaivour of SMA under cyclic loading. Comput Mater Sci 2003;23:663–74.
[19] Wang LX, Melnik RVN. Tuning vibration frequencies with shape memory alloy oscillators. In: Topping BHV, Montero G, Montenegro R, editors. Proceedings of the eighth international conference on computational structures technology. Stirlingshire, United Kingdom: Civil-Comp Press; 2006. p. 13 [paper 99, ISBN 1-905088-07-8].
[20] Falk F, Konopka P. Three-dimensional Landau theory describing the martensitic phase transformation of shape memory alloys. J Phys: Condens Matter 1990;2:61–77.
[21] Kloucek P, Reynolds DR, Seidman TI. Computational modelling of vibration damping in SMA wires. Continuum Mech Thermodyn 2004;16:495–514.
[22] Wang LX, Melnik RVN. Dynamics of shape memory alloys patches. Mater Sci Eng A 2004;378(1–2):470–4.
[23] Savi MA, de Paula AS, Lagoudas DC. Numerical investigation of an adaptive vibration absorber using SMAs. J Intell Mater Syst Struct 2011;22:67–80.
[24] Dhote RP et al. Hysteresis phenomena in SMAs by non-isothermal Ginburg–Landau models, submitted.
[25] Wang LX, Melnik RVN. Numerical model for vibration damping resulting from the first-order phase transformations. Appl Math Modell 2007;31(9):2008–18.
[26] Dhote RP et al. Microstructures of constrained shape memory alloy nanowires under thermal effects. In: Proceedings of the ASME conference on smart materials, adaptive structures and intelligent systems, vol. 1. 2010. p. 597–603.
[27] Sreekumar M, Singaperumal M, Nagarajan T, Zoppi M, Molfino R. Recent advances in nonlinear control technologies for shape memory alloy actuators. J Zhejiang Univ Sci A 2007;8(5):818–29.
[28] Li ZQ et al. Adjustable fluid dampers with SMA actuators. Smart Mater Struct 2006;15(5):1483–92.
[29] McCormick J et al. Seismic vibration control using superelastic. SMA J Eng Mater Technol – Trans ASME 2006;128(3):294–301.
[30] Liu M et al. Investigation of vibration mitigation of stay cables incorporated with superelastic SMA dampers. Smart Mater Struct 2007;16(6):2202–13.
[31] Pan Q, Cho C. The investigation of a SMA micro-damper for MEMS applications. Sensors 2007;7(9):1887–900.
[32] Zhang HS, Komvopoulos K. Thermomechanical effects on phase transformations in single-crystal Cu–Al–Ni SMA. J Mater Res 2007;22(4):994–1003.
[33] Alam MS, Youseff MA, Nehdi M. Utilizing SMA to enhance the performance and safety of civil infrastructure: a review. Can J Civil Eng 2007;34(9):1075–86.
[34] Alam MS, Nehdi M, Youseff MA. SMA-based smart RC bridges: overview of state-of-the-art. Smart Struct Syst 2008;4(3):367–89.
[35] Wang LX, Melnik RVN. Phase transformations in finite length nanowires: analysis with mesoscopic models. In: Papadrakakis M, Topping BHV, editors. Proceedings of the sixth international conference on engineering computational technology, Civil-Comp Press, Paper 139: 2008. 10 p.
[36] Zhang Y, Zhu S. A SMA-based reusable hysteretic damper for seismic hazard mitigation. Smart Mater Struct 2007;16(5):1603–13.

[37] Zhang YF, Zhu SY. Seismic response control of building structures with superelastic SMA wire dampers. J Eng Mech – ASCE 2008;134(3):240–51.

[38] Bonetti E, Fremond M, Lexcellent C. Modelling shape memory alloys. J Phys IV France 2004;115:383–90.

[39] Elhadrouz M, Ben Zineb T, Patoor E. Constitutive law for ferroelastic and ferroelectric piezoceramics. J Intell Mater Syst Struct 2005;16:221–36.

[40] Leclercq S, Lexcellent C. A general macroscopic description of the thermomechanical behaviour of shape memory alloys. J Mech Physc Solids 1996;44(6):953–80.

[41] Chen YC, Lagoudas DC. Impact induced phase transformation in shape memory alloys. J Mech Phys Solids 2000;48:275–300.

[42] Collet M, Foltete E, Lexcellent C. Analysis of the behavior of a shape memory alloy beam under dynamical loading. Eur J Mech A/Solids 2001;20:615–30.

[43] Thiebaud F, Lexcellent C, Collet M, Foltete E. Implementation of a model taking into account the asymmetry between tension and compression, the temperature effects in a finite element code for shape memory alloys structures calculations. Comput Mater Sci 2007;41(2):208–21.

[44] Melnik RVN, Roberts AJ, Thomas KA. Computing dynamics of copper-based SMA via centre manifold reduction of 3D models. Comput Mater Sci 2000;18(3–4):255–68.

[45] Melnik RVN, Roberts AJ. Thermomechanical behaviour of thermoelectric SMA actuators. J Phys IV 2001;11(PR8):515–20.

[46] Melnik RVN, Roberts AJ, Thomas KA. Coupled thermomechanical dynamics of phase transitions in shape memory alloys and related hysteresis phenomena. Mech Res Commun 2001;28(6):637–51.

[47] Melnik RVN, Roberts AJ. Computational models for materials with shape memory: towards a systematic description of coupled phenomena, Computational Science-ICCS 2002, PT II. In: Proceedings, book series: lecture notes in computer science, vol. 2330. 2002. p. 490–499.

[48] Melnik R, Wang LX. Phase-field approach to studying shape memory effects and thermomechanical properties of low dimensional nanostructures. In: Martin O, et al. editors. Advanced research in physics and engineering. Mathematics and computers in science and engineering; 2010. p. 125–130.

[49] Dhote RP, Melnik RVN, Zu J. Dynamic thermo-mechanical coupling and size effects in finite shape memory alloy nanostructures. Comput Mater Sci 2012;63:105–17.

[50] Mahapatra DR, Sutrakar VK, Melnik RVN. Temperature and stress controlled surface manipulation in Ni–Al nano-layers, Nanotech Conference & Expo 2009. In: Laudon M, Romanowicz B, editors. Technical proceedings – nanotechnology 2009: biofuels, renewable energy, coating fluidics and compact modeling, vol. 3. 2009. p. 227–30.

[51] Li DS et al. Lightweight NiTi shape memory alloy based composites with high damping capacity and high strength. J Alloys Compd 2010;490(1–2):L15–9.

[52] Melnik RVN, Roberts A. Computational models for multi-scale coupled dynamic problems. Future Generation Comput Syst 2004;20(3):453–64.

[53] Melnik RVN, Povitsky A. Wave phenomena in physics and engineering: new models, algorithms, and applications. Math Comput Simul 2004;65(4–5):299–302.

[54] Melnik RVN, Roberts AJ. Modelling nonlinear dynamics of shape-memory-alloys with approximate models of coupled thermoelasticity. Zeitschrift fur Angewandte Mathematik und Mechanik 2003;83(2):93–104.

[55] Melnik RVN, Wang L, Matus P, Rybak L. Computational aspects of conservative difference schemes for shape memory alloys applications. In: Computational Science and its Applications – ICCSA 2003, PT 2, Proceedings. Lecture Notes in computer science, vol. 2668. 2003. p. 791–800.

[56] Matus P, Melnik RVN, Wang L, Rybak I. Applications of fully conservative schemes in nonlinear thermoelasticity: modelling shape memory material. Math Comput Simul 2004;65(4–5):489–509.

[57] Wang LX, Melnik RVN. Thermomechanical waves in SMA patches under small mechanical loadings. In: Computational Science – ICCS 2004, Part 4, proceedings. Lecture notes in computer science, vol. 3039. 2004. p. 645–52.

[58] Wang LX, Melnik R. Dynamics of shape memory alloys patches with mechanically induced transformations. Discrete Contin Dyn Syst 2006;15(4):1237–52.

[59] Wang LX, Melnik RVN. Two-dimensional analysis of shape memory alloys under small loadings. Int J Multiscale Comput Eng 2006;4(2):291–304,.

[60] Wang LX, Melnik RVN. Differential–algebraic approach to coupled problems of dynamic thermoelasticity. Appl Math Mech 2006;27(9):1185–96.

[61] Wang LX, Melnik RVN. Simulation of nonlinear thermomechanical waves with an empirical low dimensional model. In: Computational science – ICCS 2005, Pt 1, proceedings. Lecture notes in computer science, vol. 3514. 2005. p. 884–91.

[62] Wang LX, Melnik RVN. Model reduction applied to square to rectangular martensitic transformations using proper orthogonal decomposition. Appl Numer Math 2007;57(5–7):510–520,.

[63] Wang LX, Melnik RVN. Low dimensional approximations to ferroelastic dynamics and hysteretic behavior due to phase transformations. J Appl Mech – Trans ASME 2010;77(3) [Art. No. 031015].

[64] Wang LX, Melnik RVN. Mechanically induced phase combination in shape memory alloys by Chebyshev collocation methods. Mater Sci Eng A 2006;438(Sp. Iss.):427–30.

[65] Wang LX, Melnik RVN. Modifying macroscale variant combinations in a two-dimensional structure using mechanical loadings during thermally induced transformation. Mater Sci Eng A 2008;481(Sp. Iss.):190–3.

[66] Wang LX, Melnik RVN. Thermo-mechanical wave propagations in shape memory alloy rod with phase transformations. Mech Adv Mater Struct 2007;14(8):665–76.

[67] Wang LX, Melnik RVN. Finite volume analysis of nonlinear thermo-mechanical dynamics of shape memory alloys. Heat Mass Transfer 2007;43(6):535–46.

[68] Mahapatra DR, Melnik RVN. Numerical simulation of phase transformations in shape memory alloy thin films. In: Computational science – ICCS 2006, Pt 2, proceedings, vol. 3992. 2006. p. 114–21.

[69] Mahapatra DR, Melnik RVN. Finite element modelling and simulation of phase transformations in shape memory alloy thin films. Int J Multiscale Comput Eng 2007;5(1):65–71.

[70] Mahapatra DR, Melnik R, A dynamic model for phase transformations in 3D samples of shape memory alloys. In: Computational science – ICCS 2005, Pt 3. Lecture series in computer science, vol. 3516. 2005. p. 25–32.

[71] Mahapatra DR, Melnik R. Three-dimensional mathematical models of phase transformation kinetics in shape memory alloys. Dyn Contin Discrete Impulsive Syst Ser B – Appl Algorithms 2005;2(Sp. Iss. SI):557–62.

[72] Mahapatra DR, Melnik RVN. Finite element analysis of phase transformation dynamics in shape memory alloys with a consistent Landau–Ginzburg free energy model. Mech Adv Mater Struct 2006;13(6):443–55.

[73] Mahapatra DR, Melnik RVN. Finite element approach to modelling evolution of 3D shape memory materials. Math Comput Simul 2007;76(1–3):141–8.

[74] Wang LX, Melnik RVN. Simulation of phase combinations in shape memory alloys patches by hybrid optimization methods. Appl Numer Math 2008;58(4):511–24.

[75] Ozbulut OI et al. GA-based optimum design of a shape memory alloy device for seismic response mitigation. Smart Mater Struct 2010;19(6) [Art. No. 065004].

[76] Wang LX, Liu R, Melnik RVN. Feedback linearization of hysteretic thermoelastic dynamics of shape memory alloy actuators with phase transformations. In: Lau AKT, Lu J, Varadan VK, Chang FK, Tu JP, Lam PM, editors. Multi-functional materials and structures, Pts 1 and 2, Advanced materials research, vol. 47–50 Part 1–2, 2008. p. 69–72.

[77] Wang LX, Melnik RVN. Control of coupled hysteretic dynamics of ferroelectric materials with a Landau-type differential model and feedback linearization. Smart Mater Struct 2009;18(7) [Art. No. 074011[.

[78] Salje EKH et al. Martensitic transformation B2-R in Ni–Ti–Fe: experimental determination of the Landau potential and quantum saturation of the order parameter. J Phys – Condens Matter 2008;20(27):275216.

[79] Niezgodka M, Sprekels J. Convergent numerical approximations of the thermomechanical phase transitions in shape memory alloys. Numer Math 1991;58:759–78.

[80] Huo Y, Muller I. Nonequilibrium thermodynamics of pseudoelasticity. Continuum Mech Therm 1993;5:163–204.

[81] Graczykowski B et al. Elastic properties of Cu–Al–Ni shape memory alloys studied by dynamic mechanical analysis. Smart Mater Struct 2010;19(1) [Art. No. 015010].

[82] Fu S, Huo Y, Muller I. Thermodynamics of pseudoelasticity an analytical approach. Acta Mech 1993;99:119.

[83] Bunber N. Landau–Ginzburg model for a deformation-driven experiment on shape memory alloys. Continuum Mech Therm 1996;8:293–308.